Mingchao Wang, Marco Ballabio, Mao Wang, Hung-Hsuan Lin, Bishnu P. Biswal, Xiaocang Han, Silvia Paasch, Eike Brunner, Pan Liu, Mingwei Chen, Mischa Bonn, Thomas Heine, Shengqiang Zhou, Enrique Cánovas, Renhao Dong, Xinliang Feng

Unveiling Electronic Properties in Metal–Phthalocyanine-Based Pyrazine-Linked Conjugated Two-Dimensional Covalent Organic Frameworks

Erstveröffentlichung in / First published in:

Journal of the American Chemical Society. 2019, 141 (42), S. 16810 – 16816. ACS Publications. ISSN 1520-5126.

DOI: https://doi.org/10.1021/jacs.9b07644

Final edited form was published in "Journal of the American Chemical Society". 2019, 141 (42), S. 16810 – 16816. ISSN 1520-5126.
https://doi.org/10.1021/jacs.9b07644

Unveiling Electronic Properties in Metal-Phthalocyanine-based Pyrazine-linked Conjugated Two-Dimensional Covalent-Organic Frameworks

Mingchao Wang[†], Marco Ballabio[‡], Mao Wang[§], Hung-Hsuan Lin[†], Bishnu P. Biswal[†], Xiaocang Han[∥], Silvia Paasch[†], Eike Brunner[†], Pan Liu[∥], Mingwei Chen[∥,▽], Mischa Bonn[‡], Thomas Heine[†,#], Shengqiang Zhou[§], Enrique Cánovas[‡,⊥]*, Renhao Dong[†]*, Xinliang Feng[†]*

[†]*Center for Advancing Electronics Dresden (cfaed) & Department of Chemistry and Food Chemistry, Technische Universität Dresden, Mommsenstrasse 4, 01062 Dresden, Germany*

[‡]*Max Planck Institute for Polymer Research, Ackermannweg 10, 55128 Mainz, Germany*

[§]*Helmholtz-Zentrum Dresden-Rossendorf, Institute of Ion Beam Physics and Materials Research, Bautzner Landstr. 400, 01328 Dresden, Germany*

[∥]*State Key Laboratory of Metal Matrix Composites and Shanghai Key Laboratory of Advanced High-temperature Materials and Precision Forming, School of Materials Science and Engineering, Shanghai Jiao Tong University, Shanghai, 200030, China*

[▽]*Department of Materials Science and Engineering, Johns Hopkins University, Baltimore, MD, 21218, USA*

[#]*Helmholtz-Zentrum Dresden-Rossendorf, Institute of Resource Ecology, Bautzner Landstr. 400, 01328 Dresden, Germany*

[⊥]*Instituto Madrileño de Estudios Avanzados en Nanociencia (IMDEA Nanociencia), Faraday 9, 28049 Madrid, Spain.*

ABSTRACT: π-Conjugated two-dimensional covalent organic frameworks (2D COFs) are emerging as a novel class of electroactive materials for (opto-)electronic and chemiresistive sensing applications. However, understanding the intricate interplay between chemistry, structure and conductivity in π-conjugated 2D COFs remains elusive. Here, we report a detailed characterization for the electronic properties of two novel samples consisting of Zn- and Cu-phthalocyanine-based pyrazine-linked 2D COFs. These 2D COFs are synthesized by condensation of metal-phthalocyanine (M=Zn and Cu) and pyrene derivatives. The obtained polycrystalline-layered COFs are *p*-type semiconductors both with a band gap of ~1.2 eV. Mobilities up to ~5 cm^2/Vs are resolved in the dc limit, which represent a lower threshold induced by charge carrier localization at crystalline grain boundaries. Hall Effect measurements (dc limit) and terahertz (THz) spectroscopy (ac limit) in combination with density functional theory (DFT) calculations demonstrate that varying metal center from Cu to Zn in the phthalocyanine moiety has a negligible effect in the conductivity (~5×10^{-7} S/cm), charge carrier density (~10^{12} cm^{-3}), charge carrier scattering rate (~3×10^{13} s^{-1}), and effective mass (~$2.3m_0$) of majority carriers (holes). Notably, charge carrier transport is found to be anisotropic, with hole mobilities being practically null in-plane and finite out-of-plane for these 2D COFs.

INTRODUCTION

Covalent-organic frameworks (COFs) belongs to a class of porous and crystalline polymers,[1] which hold promise in a plethora of applications such as chemosensing,[2] gas storage[3] and separation.[4] Conjugated two-dimensional (2D) COFs, also termed as 2D conjugated polymer frameworks, have also been rising as active semiconductors for potential applications in optoelectronics,[5] photovoltaics,[6] chemiresistive sensing[7] and (photo-)electrocatalysis[8]. To date, improved electronic properties in π-conjugated 2D COFs have been achieved by systematic engineering of the framework favoring extended conjugation,[9] e.g., by employing conjugated linkers such as carbon-carbon bonds[10] and pyrazine units.[7,11] A pyrazine-linked triphenylene-/pyrene-based 2D COF revealed a charge carrier mobility (ac limit) as high as 4.2 cm^2/Vs (measured by flash photolysis time-resolved microwave conductivity, FP-TRMC).[11a] Besides conjugated linkers, planar conjugated building blocks such as pyrene, porphyrin, hexabenzocoronene and phthalocyanine have been employed with the aim of improving mobilities.[12] For instance, a porphyrin-based 2D COF linked by imine bonds exhibited a mobility of 8.1 cm^2/Vs (estimated by FP-TRMC at room temperature).[12b] Although these results illustrate that improved charge transport properties are at reach by rational tuning of COF structures,[13] current approaches are generally unable to establish a neat relationship between the structure and electronic properties. To do so, a thorough analysis of intrinsic and extrinsic factors affecting the charge transport is highly required for π-conjugated 2D COFs where differential analysis is feasible (i.e. where changes in composition are not dramatically affecting the energy band diagram).

In this work, we introduce two novel pyrazine (**pz**)-linked metal-phthalocyanine (**MPc**)-based conjugated 2D COFs

Final edited form was published in "Journal of the American Chemical Society". 2019, 141 (42), S. 16810 – 16816. ISSN 1520-5126.
https://doi.org/10.1021/jacs.9b07644

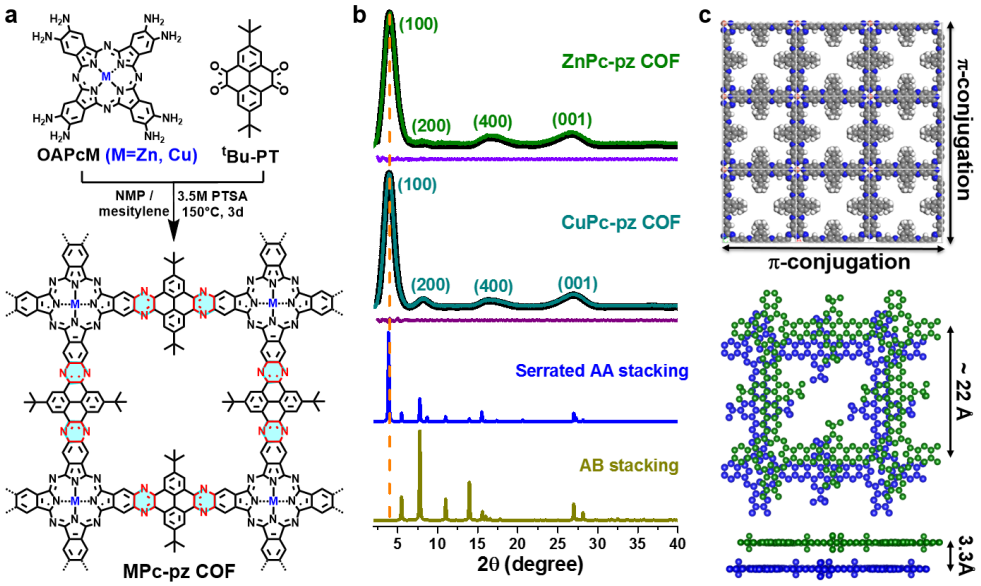

Figure 1. Design and synthesis of **MPc-pz** COF (M = Zn or Cu) with highly π-conjugated structure. (a) Schematic illustration of the condensation reaction between **OAPcM** and **^{t}Bu-PT** to form the pyrazine linkages. (b) Experimental (green line) and Pawley refined (black dotted line) PXRD pattern as well as the corresponding difference plot (violet line) of **ZnPc-pz**; experimental (dark cyan line) and Pawley refined (black dotted curve) PXRD patterns as well as the difference plot (purple line) of **CuPc-pz**; calculated PXRD patterns for serrated AA stacking (blue line) and AB stacking (dark yellow line). (c) Monolayer of **MPc-pz** (top) as well as top view (middle) and side view (down) of the serrated AA stacked structure.

(**MPc-pz**, M = Zn or Cu), that assembled as van der Waals (vdWs) layer-stacked structures. The **MPc-pz** materials were synthesized by condensation of 2,3,9,10,16,17,23,24-octaamino-phthalocyaninato metal [II] (**OAPcZn** or **OAPcCu**) and *tert*-butylpyrene-tetraone (**^{t}Bu-PT**) under solvothermal conditions. The resultant materials are found to be polycrystalline *p*-type semiconductors with band gaps of ~1.2 eV. Van der Pauw,[14] Hall effect[15], time-resolved terahertz spectroscopy (TRTS)[16] and density functional theory (DFT) calculations are employed for characterizing univocally the intrinsic and extrinsic factors determining the electronic properties of these materials. We demonstrate that for this *p*-type semiconductor, changing metal center from Cu to Zn in the phthalocyanine moiety has a negligible effect in the conductivity (~5×10^{-7} S/cm), charge density (~10^{12} cm^{-3}), charge carrier scattering rate (~3×10^{13} s^{-1}), and effective mass (~$2.3m_0$) of majority carriers (holes). Mobilities up to ~5 cm^2/Vs are resolved in the dc limit, which is limited by long range charge carrier transport across crystalline grain boundaries. Interestingly, charge transport is found to be highly anisotropic, with hole mobilities being practically null in-plane and finite out-of-plane for the developed 2D COFs. This work highlights the potential of high mobility π-conjugated 2D COFs as semiconductors for (opto-)electronics and provides a rational approach to ascertain structure-property relationships, revealing that a detailed analysis of the conductivity might offer a reliable path for designing and developing semiconducting COF materials with improved charge transport properties.

RESULTS AND DISCUSSION

Synthesis and Sample Characterization. The monomer **OAPcM (M=Zn or Cu)** was synthesized by a 3-step organic reaction route in ~40% total yield: Buchwald-Hartwig amination of 4,5-dichlorophthalonitrile, cyclization condensation and subsequent hydrolysis reaction (Scheme S3 of Supporting Information). **MPc-pz** COFs were obtained through a condensation reaction of **OAPcM** and **^{t}Bu-PT** monomers with *p*-toluenesulfonic acid (PTSA) as catalyst in 1-methyl-2-pyrrolidone (NMP)/mesitylene (2:1, v/v) heated at 150 °C in a sealed Schlenk tube for 3 days (Fig. 1a and Scheme S4, other reaction conditions seen in Table S1). The solid product was collected and washed with dimethylformamide, deionized water, methanol and dichloromethane (DCM). After Soxhlet extraction with methanol and DCM, **MPc-pz** was collected and dried under vacuum at 120 °C overnight to afford dark green powders in ~80% yield.

Powder X-ray diffraction (PXRD) analysis reveals crystalline nature for both **ZnPc-pz** and **CuPc-pz** COFs with distinct peaks at 3.98°, 8.08°, 16.63° and 26.71° (Fig. 1b, green line), and 3.97°, 8.21°, 16.67° and 26.97° (Fig. 1b, dark cyan line), respectively which are assigned to (100), (200), (400) and (001) crystallographic planes (Fig. 1b, the black lines refer to the Pawley refined pattern, for details see Section A, Supporting Information). Density functional theory (DFT) calculations (see Supporting Information for computational details and Figure S1) reveal that the experimental PXRD pattern resolved in the samples is consistent with a serrated AA stacking (Figure 1b, blue line and 1c, Figures S2-4). Notably, the *tert*-butyl groups in pyrazine moieties largely contribute to the layer-stacking conformation in these 2D COFs.[7] From the PXRD data and first-principles calculations we can conclude that both COFs are defined by square unit cells with a = b = 22.2 Å, and an inter-plane distance of ~3.30 Å for **ZnPc-pz** and **CuPc-pz**. Both COFs are polycrystalline;

Final edited form was published in "Journal of the American Chemical Society". 2019, 141 (42), S. 16810 – 16816. ISSN 1520-5126.
https://doi.org/10.1021/jacs.9b07644

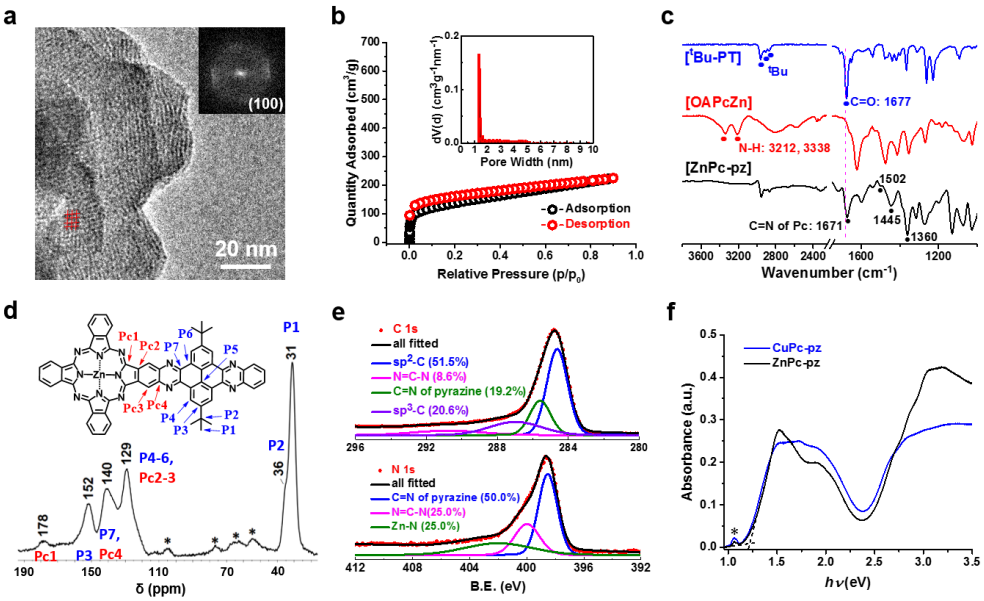

Figure 2. Morphological, structural, compositional and optical analysis of **ZnPc-pz** COF. (a) HR-TEM image. The insert is the related fast Fourier transform (FFT) analysis. The inserted red lines draw a square pattern with the unit size of ~2 nm. (b) N_2 adsorption/desorption isotherms measured at 77.3 K. The insert is the corresponding pore size distribution calculated using NLDFT method. (c) FT-IR spectra of **ZnPc-pz** COF (black), **OAPcZn** (red) and **^{t}Bu-PT** (blue). (d) Solid-state ^{13}C CP-MAS NMR spectrum. Sidebands are marked by asterisks. (e) High-resolution C*(1s)* and N*(1s)* XPS spectrum. (f) UV/vis absorption spectroscopy with $h\nu$ as horizontal axis. The optical band gaps of **ZnPc-pz** (black) and **CuPc-pz** (blue) COF were obtained as 1.20 eV and 1.18 eV, respectively. Solvent peaks are marked by an asterisk.

Scherrer's equation applied to the experimental PXRD patterns reveals averaged crystal sizes of ~7.9 nm and ~8.0 nm for **ZnPc-pz and CuPc-pz** COF samples, respectively.

Transmission electron microscopy (TEM) studies provide further evidence of crystalline grains with an estimated diameter of ~10 nm in the case of **MPc-pz** (Figure S5). High-resolution TEM (HRTEM) imaging and the related fast Fourier transform (FFT) analysis further demonstrate a square unit cell with lattice parameters, a = b = ~2.0 nm (Figure 2a and Figure S6), which is in good agreement with PXRD and DFT results. Field-emission scanning electron microscopy (FE-SEM) images show aggregated particles for **ZnPc-pz** and **CuPc-pz** (Figures S7 and 8). The corresponding energy-dispersive X-ray (EDX) spectroscopies suggest a homogeneous distribution of N and C elements and metal centers (Zn or Cu) throughout the samples (Figures S9 and 10).

The porosity of these samples was determined by low-pressure nitrogen adsorption measurements at 77.3 K. The Brunauer-Emmett-Teller (BET) surface areas of **ZnPc-pz** and **CuPc-pz** were found to be 487.4 and 458.9 $m^2 \cdot g^{-1}$ respectively (Figure 2b, Figures S11 and 12). The pore size distribution calculated by the non-local density functional theory (NLDFT) method[17] revealed an average pore size of ~1.4 nm (Figure 2b, insert), which is slightly smaller than the lattice parameters determined from the PXRD. The pore size reduction could be ascribed to pores that are partially blocked by the *tert*-butyl groups.

The formation of desired COF network via successful condensation reaction between the **OAPcM** and **^{t}Bu-PT** monomers was corroborated by Fourier-transform infrared (FT-IR) spectroscopy and cross-polarization magic-angle spinning (CP-MAS) nuclear magnetic resonance (NMR) spectroscopy. The formation of the pyrazine linkages in **ZnPc-pz** was evident by the appearance of C=N stretching vibrations at 1502, 1445, and 1360 cm^{-1} as well as the disappearance of the vibrational bands related with amino groups (3212 and 3338 cm^{-1}) and keto units (1677 cm^{-1}) of the starting monomers (Figure 2c). Solid-state ^{1}H NMR spectroscopy of **ZnPc-pz** provided two proton signals originating from the phthalocyanine macrocycle and the *tert*-butyl group at 8.0 and 1.2 parts per million (ppm), respectively (Figure S13a). The ^{13}C CP-MAS NMR spectroscopy showed six signals at 178, 152, 140, 129, 36 and 33 ppm, which can be assigned to the Pc1, P3, P7 and Pc4, P4-6 and Pc2-3, P2, P1 carbon atoms from the phthalocyanine (Pc)- and pyrene (P)-units of **ZnPc-pz** respectively (Figure 2d and Figure S13b). The signal of P7 and Pc4 at 140 ppm further confirms the formation of the pyrazine linkages. Analogous results were obtained by FT-IR and solid-state ^{1}H- and ^{13}C-NMR spectra for **CuPc-pz** sample (Figures S14 and 15). X-ray photoelectron spectroscopy (XPS) measurement reveals the presence of C *1s*, N *1s* and Zn *2p* core levels in **ZnPc-pz** (Figure 2e and Figure S16). Deconvolution of the C(*1s*) signal generates peaks at 284, 286, 287 and 292 eV, attributable to the sp^2 carbon-carbon bond, carbon-nitrogen bond of pyrazine linkage, sp^3 carbon-carbon bond and N=C-N bond with the corresponding peak areas of 51.5%, 19.2%, 20.6% and 8.6%,[18] which agrees well with the expected structural composition of 2D COFs (Figure 2e, top). The high-resolution N(*1s*) spectrum displays peaks at 397, 400 and 402 eV, perfectly assigned to carbon-nitrogen bond of pyrazine linkage (50.0%), N=C-N bond (25.0%) and zinc-nitrogen bond (25.0%), respectively (Figure 2e, down). Moreover,

Final edited form was published in "Journal of the American Chemical Society". 2019, 141 (42), S. 16810 – 16816. ISSN 1520-5126.
https://doi.org/10.1021/jacs.9b07644

zinc(*2p*) XPS spectrum shows two sets of peaks with binding energies of 1021 eV and 1044 eV for Zn *2p*3/2 and Zn *2p*1/2, respectively, which indicates the presence of Zn(II) species. The XPS survey spectrum also reveals the element composition of C, N and Cu in **CuPc-pz** (Figure S17).

Thermal and Chemical Stability. The thermal stability of **ZnPc-pz** and **CuPc-pz** COFs was examined using thermogravimetric analysis (TGA) and variable-temperature XRD measurements. Both COFs exhibited no significant weight loss up to ~310 °C under argon atmosphere (Figure S18). Furthermore, PXRD patterns were invariant as a function of temperature (cooling the sample from room temperature to 100 K, Figure S19). Chemical stability was performed by soaking COF powders in different solvents for 24 h at room temperature including methanol, tetrahydrofuran, DCM, hexane and acetone as well as in 1 M HCl and 1 M KOH aqueous solutions.[19] Comparison of the PXRD patterns and FT-IR spectra of COFs before and after the treatment demonstrated the integrity of the pyrazine linkages and the retention of crystallinity for both samples (Figures S20 and 21).

Optical and Electrochemical Properties. The UV/Vis spectra of the dispersions of **MPc-pz** in dimethyl sulfoxide reveal that the samples are characterized by direct optical band gaps of ~1.20 eV and ~1.18 eV for **ZnPc-pz** and **CuPc-pz**, respectively (Figure 2f, also see Tauc plots of $(Ahv)^2$ vs. *hv*, Figure S23). Figures S22 and 23 compare the absorbance of **OAPcM** monomers and COF samples; the Soret-bands of COFs are red shifted by ~35 nm and the main broad absorption of Q bands is red shifted by ~100 nm, an effect attributable to the extended conjugation.[20] Cyclic voltammetry (CV) measurements were also performed by depositing COF powders on an electrode in acetonitrile and demonstrated electrochemical energy gaps of ~1.07 eV and ~1.06 eV for **ZnPc-pz** and **CuPc-pz**, respectively (Figure S24, Table S2).

DC Conductivity in MPc-pz COF. We conducted Hall Effect measurements on the developed COFs to characterize the components defining the conductivity (mobility and doping). The measurements reveal that **ZnPc-pz** and **CuPc-pz** samples are *p*-type semiconductors (Figure 3a) with inferred charge carrier densities (*p*-type doping) of $9.1(\pm0.3)\times10^{11}$ cm^{-3} and $2.3(\pm0.7)\times10^{12}$ cm^{-3}, respectively, and Hall mobility estimates at room temperature in the dc limit of 4.8±0.7 cm^2/Vs and 0.9±0.2 cm^2/Vs, respectively. Notably, the mobility of ~5 cm^2/Vs obtained by Hall Effect measurements represent to the best of our knowledge a record device-relevant dc mobility value when compared to the state-of-art reports of semiconducting COF samples (Table S3). From these numbers we infer similar conductivities of 7.0×10^{-7} and 3.3×10^{-7} S/cm for Zn- and Cu-phthalocyanine-based samples, respectively (Table S4). We also performed electrical dc conductivity measurements as a function of temperature (T) using the van der Pauw method[14] on COF powders pressed into pellets with an average thickness of ~0.3 mm (Figure S25a). The compressed COF pellets did not reveal any distinct changes on crystal nano-structure as proved by PXRD (Figures S25b-d, 26 and 27). Linear current-voltage (I-V) curves for **ZnPc-pz** and **CuPc-pz** samples were obtained at room temperature indicating ohmic behavior (Figures S28 and 29). Both samples revealed a typical semiconducting drop for the conductivity upon sample cooling (Figure 3b for **ZnPc-pz;** and SI for **CuPc-pz**), with almost identical activation energies for both samples (0.34 ±0.1 eV, see inset Fig. 3b and Figure S29e). Based on the above Hall Effect dc conductivity measurements, the metal center seems irrelevant in terms of doping, however a slightly better performance for **ZnPc-pz** when compared with **CuPc-pz** could be concluded in terms of mobility. A critical question arises then: are these differences intrinsic (induced by metal center nature) or extrinsic (e.g. induced by sample history)? To reveal whether the mobility (μ) is truly improved in the Zn-phthalocyanine-based sample we determined independently the parameters defining it ($\mu = q^*\tau/m^*$), that is charge carrier effective mass (m^*) and scattering rate (τ) by DFT calculations and time-resolved terahertz (THz) spectroscopy respectively (see below).

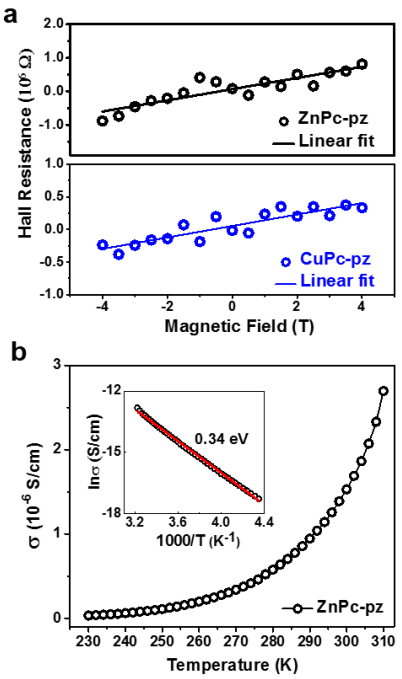

Figure 3. (a) Hall effect measurements of **ZnPc-pz** (black) and **CuPc-pz** COF (blue) at 300 K. (b) Variable-temperature electrical conductivity of **ZnPc-pz** via van der Pauw method. The insert is the plot of natural logarithm of conductivity ($ln\sigma$) as a function of inverse temperature (1000/T).

Energy Band Diagrams and Effective Mass Estimates. DFT was employed to calculate the energy band diagram for **ZnPc-pz** and **CuPc-pz** single-layer and layered 2D COFs (lattice parameters seen in Tables S5 and S6). The electronic band structure and the projected density of states (PDOS) for the **ZnPc-pz** and **CuPc-pz** monolayers are shown in Figure 4a and c. Both samples are semiconducting, and reveal an almost dispersionless conduction band (CB) and valence band (VB), implying that in-plane charge transport for monolayers is practically null owing to an extremely large effective mass for charge carriers. To take a closer look, the electron density of valence band maximum (VBM) and conduction band minimum (CBM) are illustrated in Figures S30 and S31. The π-electrons both in **ZnPc-pz** and **CuPc-pz** are trapped within the **MPc-pz** moiety. The localization of electron density causes flat bands and thus low in-plane charge transport. Notably, the situation changes for stacked COF

Final edited form was published in "Journal of the American Chemical Society". 2019, 141 (42), S. 16810 – 16816. ISSN 1520-5126.
https://doi.org/10.1021/jacs.9b07644

layers, where we observe appreciable dispersion of the band structure. For the serrated AA stacking the band gap of **ZnPc-pz** is narrowed to ~0.6 eV with respect to the monolayer (Figure 4b), as result of the band dispersion and an effect due to the interlayer π-π interaction. The band diagram reveals anisotropic transport in the stacked geometry, with a small in-plane and finite out-of-plane mobility as dictated by their effective masses (Table S7). The averaged out-of-plane carrier effective masses calculated from the band structure for serrated AA-stacked samples are m_h*=2.3m_0 and m_e*=4.7m_0 for holes and electrons respectively (Table S7). For **CuPc-pz** sample based on serrated AA stacking the band gap reduces as well when compared with monolayer from ~0.8 eV to ~0.55 eV (Figures 4c and d), this effect can be similarly attributed to interlayer π-π interaction. Once more, the energy band diagram reveals anisotropic transport. The corresponding carrier effective masses in serrated AA-stacked **CuPc-pz** are m_h*=2.3m_0 and m_e*>>>2.3m_0 for holes and electrons respectively (Table S7).

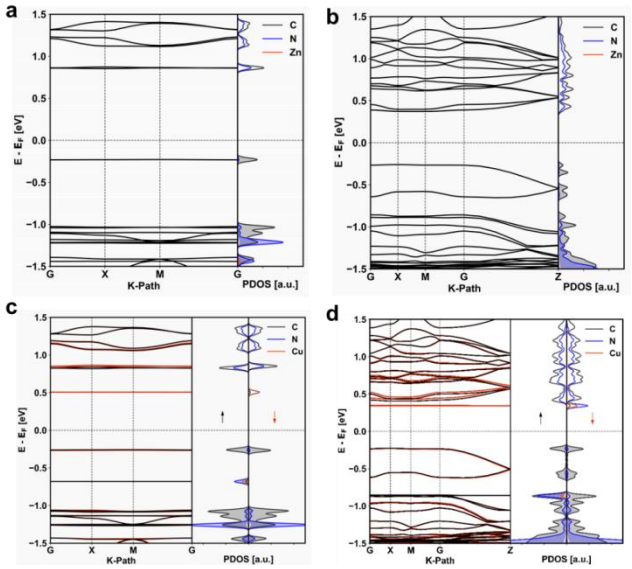

Figure 4. Electronic band structures (left panel) and projected density of states (PDOS) (right panel) of **MPc-pz** COF. (a) Monolayer and (b) serrated AA stacked multilayers of **ZnPc-pz**; (c) monolayer and (d) serrated AA stacked multilayers of **CuPc-pz**.

DFT results reveal that effective masses for hole majority carriers are identical for both samples, i.e., independent of metal center substitution. As such case, the inferred difference in hole Hall-mobilities (~4.8±0.7 cm^2/Vs and 0.9±0.2 cm^2/Vs for Zn- and Cu-phthalocyanine-based samples) must be attributed to different scattering mechanisms operating in both samples, either associated with intrinsic (associated with metal center nature) or extrinsic (e.g. due to grain boundary scattering) factors.

Time-Resolved THz Spectroscopy in MPc-pz COF. We performed time-resolved THz spectroscopy (TRTS) to analyze the photo-conductivity as a function of frequency in the samples; from this dependence it is possible to infer the free carrier scattering rates (the average time between collisions for a free charge carrier), a parameter that codetermines, together with the effective mass, the charge carrier mobility (μ=q*τ/m*). Figures 5a and 5c show the real part of the photoconductivity as a function of time, for ~200-micron thick **ZnPc-pz** and **CuPc-pz** samples (300 μJ/cm^2 800 nm pump excitation, ~1 THz probe center frequency and ~1 THz bandwidth). Carrier dynamics inferred for both samples are consistent with the ultrafast (sub-*ps*) formation of quasi-free carriers that undergo rapid trapping and/or localization within the samples.

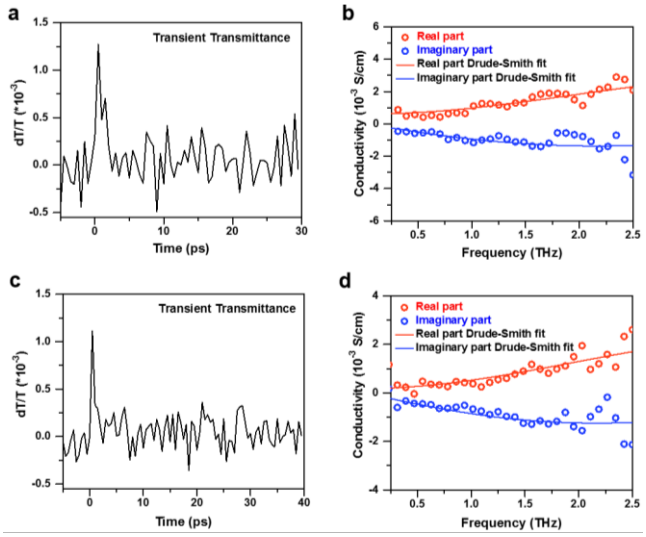

Figure 5. Time-resolved terahertz spectroscopy (TRTS) of **ZnPc-pz** (a and b) and **CuPc-pz** COF (c and d).

Figures 5b and 5d show the real and imaginary conductivity components as a function of frequency at the peak conductivity (0.5 ps after pump excitation) for **ZnPc-pz** and **CuPc-pz** COF samples, in both cases, the data can be described well by the Drude-Smith model (DS model, shown as solid lines in Figures 5b and 5d, see Methods). This phenomenological model for carrier transport is commonly employed to describe free charge carrier motion constrained by backscattering; backscattering typically occurs at grain boundaries, and is quantified within the model by a parameter c that ranges between 0 (no backscattering) and -1 (preferential backscattering). The good DS fit to the data is consistent with the polycrystalline nature for the analyzed samples, where long-range dc charge transport is impeded by the grain boundaries. The data is best described using the DS model by 30±4 *fs* average scattering times for both samples. This observation indicates that different metal centers (M=Zn and Cu) at different metal-phthalocyanine COF moieties do not affect carrier motion in the samples. DFT calculations are fully consistent with this result revealing that metal centers do not contribute to the PDOS in the VB for both samples. The only noticeable change between the DS fits come from the inferred backscattering parameters, with c parameters of -0.91±0.02 and -0.97±0.02 for **ZnPc-pz** and **CuPc-pz** COF samples. Provided that the c parameter weights the dc mobility as (μ=q*τ/m*[1+c]), and taking into account the hole effective mass estimated by DFT for both samples (m_h*=2.3m_0), we obtain mobilities of ~2.0 cm^2/Vs and ~0.7 cm^2/Vs for **ZnPc-pz** and **CuPc-pz** COF, in good agreement with the trend obtained from the hole Hall mobility estimates. These results demonstrate

Final edited form was published in "Journal of the American Chemical Society". 2019, 141 (42), S. 16810 – 16816. ISSN 1520-5126.
https://doi.org/10.1021/jacs.9b07644

that metal center (Cu or Zn) in the phthalocyanine moiety has a negligible effect in the mobility, rather extrinsic changes in boundary scattering are responsible for the observed differences. Note that differences in boundary scattering are not necessarily directly related with particle grain size (which is the same for both samples) but with the width and height of depletion regions established between crystalline domains (that are modulated by interfacial chemistry).

CONCLUSION

In summary, we have presented a detailed characterization of two novel π-conjugated 2D COFs consisting of Zn- and Cu-phthalocyanine macrocycles and pyrazine-linkages. The obtained polycrystalline layered 2D COFs (**ZnPc-pz** and **CuPc-pz**) are *p*-type semiconductors. Hole mobilities up to ~5 cm^2/Vs and intrinsic conductivity as high as $\sim 5\times10^{-7}$ S/cm are resolved in the dc limit, a figure constrained by charge carrier localization at crystalline grain boundaries. The two COF samples are structurally, morphologically and electronically identical, allowing us to determine the effect of phthalocyanine metal centers on the COFs electronic properties. Our results demonstrate that changing the metal center from Cu to Zn in the phthalocyanine moiety has a negligible effect in the electrical properties of the samples. Notably, charge carrier transport is found to be anisotropic, with hole mobilities being practically null in-plane and finite out-of-plane for these 2D COFs. Thus, this work highlights the potential of high-mobility π-conjugated 2D COFs as semiconductors for (opto-)electronics. We also unveil a reliable structure-electronic property relationship by multi-scale dc and ac measurements, which will shed light on further developing promising COF-based semiconductors for superior device performance.

ASSOCIATED CONTENT

Supporting Information

The Supporting Information is available free of charge on the ACS Publications website. Synthetic details, characterization, modelling, and conductivity measurements, and THz experiments (PDF).

AUTHOR INFORMATION

Corresponding Author

enrique.canovas@imdea.org
renhao.dong@tu-dresden.de
xinliang.feng@tu-dresden.de

Notes

The authors declare no competing interests.

ACKNOWLEDGMENT

We thank financial support from EU Graphene Flagship, ERC Consolidator Grant (T2DCP), Coordination Networks: Building Blocks for Functional Systems (SPP 1928, COORNET) as well as the German Science Council, Center of Advancing Electronics Dresden, EXC1056, (cfaed) and OR 349/1. We acknowledge Dresden Center for Nanoanalysis (DCN) at TUD; Dr. Philipp Schlender, Dr. Konrad Schneider (Leibniz Institute for Polymer Research, IPF, Dresden), Dr. Tilo Lübken and Mr. Friedrich Schwotzer for the use of facilities. We also appreciate Mr. Ji Ma, Dr. Haixia Zhong, and Ms. Yu Zhang (UvA) for the MS, SEM and XPS analysis, respectively. We thank Mr. Chi Xu (HZDR), Dr. Chongqing Yang and Dr. Zhongquan Liao (IKTS) for the helpful discussions. Prof. T. Heine and Hung-Hsuan Lin acknowledge the Centre for Information Services and High-Performance Computing (ZIH) in Dresden, Germany for the provided computational resources.

REFERENCES

(1) (a) Côté, A. P.; Benin, A. I.; Ockwig, N. W.; O'Keeffe, M.; Matzger, A. J.; Yaghi, O. M. Porous, Crystalline, Covalent Organic Frameworks. *Science* **2005,** *310*, 1166-1170. (b) Xu, F.; Xu, H.; Chen, X.; Wu, D.; Wu, Y.; Liu, H.; Gu, C.; Fu, R.; Jiang, D. Radical Covalent Organic Frameworks: A General Strategy to Immobilize Open-Accessible Polyradicals for High-Performance Capacitive Energy Storage. *Angew. Chem. Int. Ed.* **2015,** *54*, 6814-6818. (c) Lu, S.; Hu, Y.; Wan, S.; McCaffrey, R.; Jin, Y.; Gu, H.; Zhang, W. Synthesis of Ultrafine and Highly Dispersed Metal Nanoparticles Confined in a Thioether-Containing Covalent Organic Framework and Their Catalytic Applications. *J. Am. Chem. Soc.* **2017,** *139*, 17082-17088. (d) Haase, F.; Troschke, E.; Savasci, G.; Banerjee, T.; Duppel, V.; Dörfler, S.; Grundei, M. M. J.; Burow, A. M.; Ochsenfeld, C.; Kaskel, S.; Lotsch, B. V. Topochemical Conversion of an Imine- into a Thiazole-linked Covalent Organic Framework Enabling Real Structure Analysis. *Nat. Commun.* **2018,** *9*, 2600. (e) Ma, T.; Kapustin, E. A.; Yin, S. X.; Liang, L.; Zhou, Z.; Niu, J.; Li, L.-H.; Wang, Y.; Su, J.; Li, J.; Wang, X.; Wang, W. D.; Wang, W.; Sun, J.; Yaghi, O. M. Single-Crystal X-ray Diffraction Structures of Covalent Organic Frameworks. *Science* **2018,** *361*, 48-52.

(2) (a) Dalapati, S.; Jin, S.; Gao, J.; Xu, Y.; Nagai, A.; Jiang, D. An Azine-Linked Covalent Organic Framework. *J. Am. Chem. Soc.* **2013,** *135*, 17310-17313. (b) Das, G.; Biswal, B. P.; Kandambeth, S.; Venkatesh, V.; Kaur, G.; Addicoat, M.; Heine, T.; Verma, S.; Banerjee, R. Chemical Sensing in Two Dimensional Porous Covalent Organic Nanosheets. *Chem Sci* **2015,** *6*, 3931-3939.

(3) (a) Furukawa, H.; Yaghi, O. M. Storage of Hydrogen, Methane, and Carbon Dioxide in Highly Porous Covalent Organic Frameworks for Clean Energy Applications. *J. Am. Chem. Soc.* **2009,** *131*, 8875-8883. (b) Han, S. S.; Furukawa, H.; Yaghi, O. M.; Goddard, W. A. Covalent Organic Frameworks as Exceptional Hydrogen Storage Materials. *J. Am. Chem. Soc.* **2008,** *130*, 11580-11581.

(4) Ding, S.-Y.; Dong, M.; Wang, Y.-W.; Chen, Y.-T.; Wang, H.-Z.; Su, C.-Y.; Wang, W. Thioether-Based Fluorescent Covalent Organic Framework for Selective Detection and Facile Removal of Mercury(II). *J. Am. Chem. Soc.* **2016,** *138*, 3031-3037.

(5) (a) Feng, X.; Ding, X.; Jiang, D. Covalent Organic Frameworks. *Chem. Soc. Rev.* **2012,** *41*, 6010-6022. (b) Ding, S. Y.; Wang, W. Covalent Organic Frameworks (COFs): from Design to Applications. *Chem. Soc. Rev.* **2013,** *42*, 548-568.

(6) (a) Dogru, M.; Handloser, M.; Auras, F.; Kunz, T.; Medina, D.; Hartschuh, A.; Knochel, P.; Bein, T. A Photoconductive Thienothiophene-based Covalent Organic Framework Showing Charge Transfer towards Included Fullerene. *Angew. Chem. Int. Ed.* **2013,** *52*, 2920-2924. (b) Wu, C.; Liu, Y.; Liu, H.; Duan, C.; Pan, Q.; Zhu, J.; Hu, F.; Ma, X.; Jiu, T.; Li, Z.; Zhao, Y. Highly Conjugated Three-Dimensional Covalent Organic Frameworks Based on Spirobifluorene for Perovskite Solar Cell Enhancement. *J. Am. Chem. Soc.* **2018,** *140*, 10016-10024.

(7) Meng, Z.; Stolz, R. M.; Mirica, K. A. Two-Dimensional Chemiresistive Covalent Organic Framework with High Intrinsic Conductivity. *J. Am. Chem. Soc.* **2019,** *141*, 11929-11937.

(8) (a) Lin, S.; Diercks, C. S.; Zhang, Y.-B.; Kornienko, N.; Nichols, E. M.; Zhao, Y.; Paris, A. R.; Kim, D.; Yang, P.; Yaghi, O. M.; Chang, C. J. Covalent Organic Frameworks Comprising Cobalt Porphyrins for Catalytic CO2 Reduction in Water. *Science* **2015,** *349*, 1208-1213. (b) Sick, T.; Hufnagel, A. G.; Kampmann, J.; Kondofersky, I.; Calik, M.; Rotter, J. M.; Evans, A.; Döblinger, M.; Herbert, S.; Peters, K.; Böhm, D.; Knochel, P.; Medina, D. D.; Fattakhova-Rohlfing, D.; Bein, T. Oriented Films of Conjugated 2D Covalent Organic Frameworks as Photocathodes for Water Splitting. *J. Am. Chem. Soc.* **2018,** *140*, 2085-2092. (c) Biswal, B. P.; Vignolo-González, H. A.; Banerjee, T.; Grunenberg, L.; Savasci, G.; Gottschling, K.; Nuss, J.; Ochsenfeld, C.; Lotsch, B. V. Sustained Solar H2 Evolution from a Thiazolo[5,4-d]thiazole-Bridged Covalent Organic Framework and Nickel-Thiolate Cluster in Water. *J. Am. Chem. Soc.* **2019,** *141*, 11082−11092.

(9) (a) Jin, Y.; Hu, Y.; Zhang, W. Tessellated Multiporous Two-Dimensional Covalent Organic Frameworks. *Nat. Rev. Chem.* **2017,** *1*,

Final edited form was published in "Journal of the American Chemical Society". 2019, 141 (42), S. 16810 – 16816. ISSN 1520-5126.
https://doi.org/10.1021/jacs.9b07644

0056. (b) Medina, D. D.; Sick, T.; Bein, T. Photoactive and Conducting Covalent Organic Frameworks. *Adv. Energy Mater.* **2017,** *7*, 1700387. (c) Dong, R.; Zhang, T.; Feng, X. Interface-Assisted Synthesis of 2D Materials: Trend and Challenges. *Chem. Rev.* **2018,** *118*, 6189-6235.

(10) (a) Liu, W.; Luo, X.; Bao, Y.; Liu, Y. P.; Ning, G. H.; Abdelwahab, I.; Li, L.; Nai, C. T.; Hu, Z. G.; Zhao, D.; Liu, B.; Quek, S. Y.; Loh, K. P. A Two-Dimensional Conjugated Aromatic Polymer via C-C Coupling Reaction. *Nat. Chem.* **2017,** *9*, 563-570. (b) Zhuang, X.; Zhao, W.; Zhang, F.; Cao, Y.; Liu, F.; Bi, S.; Feng, X. A Two-Dimensional Conjugated Polymer Framework with Fully sp2-Bonded Carbon Skeleton. *Polym. Chem.* **2016,** *7*, 4176-4181. (c) Jin, E.; Asada, M.; Xu, Q.; Dalapati, S.; Addicoat, M. A.; Brady, M. A.; Xu, H.; Nakamura, T.; Heine, T.; Chen, Q.; Jiang, D. Two-Dimensional sp2 Carbon–Conjugated Covalent Organic Frameworks. *Science* **2017,** *357*, 673-676.

(11) (a) Guo, J.; Xu, Y.; Jin, S.; Chen, L.; Kaji, T.; Honsho, Y.; Addicoat, M. A.; Kim, J.; Saeki, A.; Ihee, H.; Seki, S.; Irle, S.; Hiramoto, M.; Gao, J.; Jiang, D. Conjugated Organic Framework with Three-Dimensionally Ordered Stable Structure and Delocalized pi Clouds. *Nat. Commun.* **2013,** *4*, 2736. (b) Mahmood, J.; Lee, E. K.; Jung, M.; Shin, D.; Jeon, I. Y.; Jung, S. M.; Choi, H. J.; Seo, J. M.; Bae, S. Y.; Sohn, S. D.; Park, N.; Oh, J. H.; Shin, H. J.; Baek, J. B. Nitrogenated Holey Two-Dimensional Structures. *Nat. Commun.* **2015,** *6*, 6486.

(12) (a) Spitler, E. L.; Dichtel, W. R. Lewis Acid-Catalysed Formation of Two-Dimensional Phthalocyanine Covalent Organic Frameworks. *Nat. Chem.* **2010,** *2*, 672-677. (b) Wan, S.; Gándara, F.; Asano, A.; Furukawa, H.; Saeki, A.; Dey, S. K.; Liao, L.; Ambrogio, M. W.; Botros, Y. Y.; Duan, X.; Seki, S.; Stoddart, J. F.; Yaghi, O. M. Covalent Organic Frameworks with High Charge Carrier Mobility. *Chem. Mater.* **2011,** *23*, 4094-4097. (c) Calik, M.; Auras, F.; Salonen, L. M.; Bader, K.; Grill, I.; Handloser, M.; Medina, D. D.; Dogru, M.; Löbermann, F.; Trauner, D.; Hartschuh, A.; Bein, T. Extraction of Photogenerated Electrons and Holes from a Covalent Organic Framework Integrated Heterojunction. *J. Am. Chem. Soc.* **2014,** *136*, 17802-17807. (d) Dalapati, S.; Addicoat, M.; Jin, S.; Sakurai, T.; Gao, J.; Xu, H.; Irle, S.; Seki, S.; Jiang, D. Rational Design of Crystalline Supermicroporous Covalent Organic Frameworks with Triangular Topologies. *Nat. Commun.* **2015,** *6*, 7786. (e) Biswal, B. P.; Valligatla, S.; Wang, M.; Banerjee, T.; Saad, N. A.; Mariserla, B. M. K.; Chandrasekhar, N.; Becker, D.; Addicoat, M.; Senkovska, I.; Berger, R.; Rao, D. N.; Kaskel, S.; Feng, X. Nonlinear Optical Switching in Regioregular Porphyrin Covalent Organic Frameworks. *Angew. Chem. Int. Ed.* **2019,** *58*, 6896-6900.

(13) (a) Cai, S.-L.; Zhang, Y.-B.; Pun, A. B.; He, B.; Yang, J.; Toma, F. M.; Sharp, I. D.; Yaghi, O. M.; Fan, J.; Zheng, S.-R.; Zhang, W.-G.; Liu, Y. Tunable Electrical Conductivity in Oriented Thin Films of Tetrathiafulvalene-based Covalent Organic Framework. *Chem. Sci.* **2014,** *5*, 4693-4700. (b) Colson, J. W.; Dichtel, W. R. Rationally Synthesized Two-Dimensional Polymers. *Nat. Chem.* **2013,** *5*, 453-465. (c) Evans, A. M.; Parent, L. R.; Flanders, N. C.; Bisbey, R. P.; Vitaku, E.; Kirschner, M. S.; Schaller, R. D.; Chen, L. X.; Gianneschi, N. C.; Dichtel, W. R. Seeded Growth of Single-Crystal Two-Dimensional Covalent Organic Frameworks. *Science* **2018,** *361*, 52-57. (d) Mandal, A. K.; Mahmood, J.; Baek, J.-B. Two-Dimensional Covalent Organic Frameworks for Optoelectronics and Energy Storage. *ChemNanoMat* **2017,** *3*, 373-391.

(14) Van der Pauw, L. J. A Method of Measuring Specific Resistivity and Hall Effect of Discs of Arbitrary Shape. *Philips Res. Reports* **1958,** *13*, 1-9.

(15) Podzorov, V.; Menard, E.; Rogers, J. A.; Gershenson, M. E. Hall Effect in the Accumulation Layers on the Surface of Organic Semiconductors. *Phys. Rev. Lett.* **2005,** *95*, 226601.

(16) (a) Ulbricht, R.; Hendry, E.; Shan, J.; Heinz, T. F.; Bonn, M. Carrier Dynamics in Semiconductors Studied with Time-Resolved Terahertz Spectroscopy. *Rev. Mod. Phys.* **2011,** *83*, 543-586. (b) Dong, R.; Han, P.; Arora, H.; Ballabio, M.; Karakus, M.; Zhang, Z.; Shekhar, C.; Adler, P.; Petkov, P. S.; Erbe, A.; Mannsfeld, S. C. B.; Felser, C.; Heine, T.; Bonn, M.; Feng, X.; Cánovas, E. High-Mobility Band-Like Charge Transport in a Semiconducting Two-Dimensional Metal–Organic Framework. *Nat. Mater.* **2018,** *17*, 1027-1032.

(17) Groen, J. C.; Peffer, L. A. A.; Pérez-Ramírez, J. Pore Size Determination in Modified Micro- and Mesoporous Materials. Pitfalls and Limitations in Gas Adsorption Data Analysis. *Microporous and Mesoporous Mater.* **2003,** *60*, 1-17.

(18) Biesinger, M. C.; Payne, B. P.; Grosvenor, A. P.; Lau, L. W. M.; Gerson, A. R.; Smart, R. S. C. Resolving Surface Chemical States in XPS Analysis of First Row Transition Metals, Oxides and Hydroxides: Cr, Mn, Fe, Co and Ni. *Appl. Surf. Sci.* **2011,** *257*, 2717-2730.

(19) Guan, X.; Li, H.; Ma, Y.; Xue, M.; Fang, Q.; Yan, Y.; Valtchev, V.; Qiu, S. Chemically Stable Polyarylether-based Covalent Organic Frameworks. *Nat. Chem.* **2019,** *11*, 587-594.

(20) Brédas, J.-L.; Cornil, J.; Heeger, A. J. The Exciton Binding Energy in Luminescent Conjugated Polymers. *Adv. Mater.* **1996,** *8*, 447-452.